



PCCP

Carbon Dioxide Adsorption to UiO-66: Theoretical Analysis of Binding Energy and NMR properties

Journal:	<i>Physical Chemistry Chemical Physics</i>
Manuscript ID	CP-ART-08-2023-004033.R1
Article Type:	Paper
Date Submitted by the Author:	28-Sep-2023
Complete List of Authors:	Atsumi, Michiko; University of Oslo, Chemistry Zheng, Jia-Jia; National Center for Nanoscience and Technology, Laboratory of Theoretical and Computational Nanoscience Tellgren, Erik; Centre for Theoretical and Computational Chemistry, Hylleraas Centre for Quantum Molecular Sciences, Department of Chemistry Sakaki, Shigeyoshi; Kyoto University, Fukui Institute for Fundamental Chemistry Helgaker, Trygve; University of Oslo, Department of Chemistry

SCHOLARONE™
Manuscripts

Carbon Dioxide Adsorption to UiO-66: Theoretical Analysis of Binding Energy and NMR properties

Michiko Atsumi,[†] Jia-Jia Zheng,[‡] Erik Tellgren,[†] Shigeyoshi Sakaki,^{*,§}
and Trygve Helgaker^{*,†}

[†]*Hylleraas Centre for Quantum Molecular Sciences, Department of Chemistry,
University of Oslo, Box 1033, N-0315, Norway*

[‡]*Laboratory of Theoretical and Computational Nanoscience, CAS Center for
Excellence in Nanoscience, National Center for Nanoscience and Technology, Chinese
Academy of Sciences, No.11 Zhong Guan Cun Bei Yi Tiao, Beijing 100190, China*

[§]*Institute for Integrated Cell-Material Sciences, Kyoto University, Rhom Plaza
R312, Kyoto-daigaku-Katsura, Nishikyo-ku, Kyoto 615-8146, Japan*

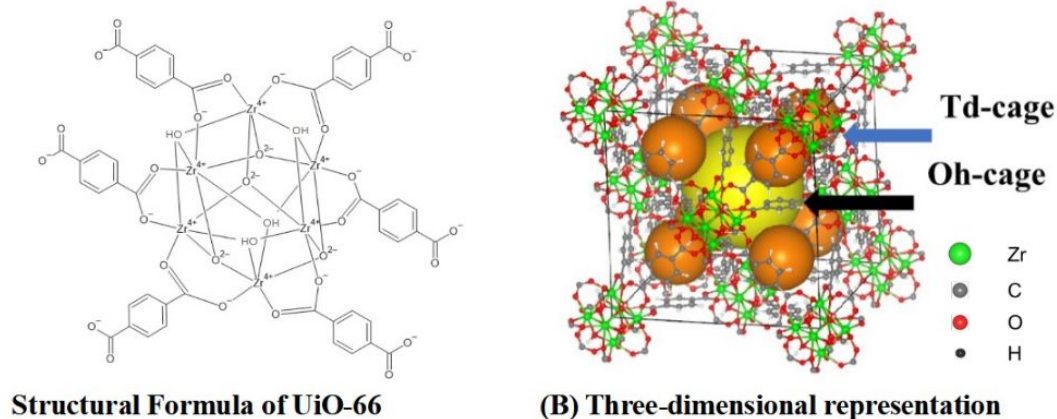
E-mail: sakaki.shigeyoshi.47e@st.kyoto-u.ac.jp; t.u.helgaker@kjemi.uio.no

Abstract: UiO-66 is one of the most valuable metal organic frameworks because of its excellent adsorption capability for gas molecules and its high stability towards water. Herein we investigated adsorption of carbon dioxide (CO_2), acetone, and methanol to infinite UiO-66 using DFT calculations on an infinite system under periodic-boundary condition and post-Hartree-Fock (SCS-MP2 and MP2.5) calculations on cluster models. Three to four molecules are adsorbed at each of four $\mu\text{-OH}$ groups bridging three Zr atoms in one unit cell (named Site I). Six molecules are adsorbed around three pillar ligands, where the molecule is loosely surrounded by three terephthalate ligands (named Sites II). Also, six molecules are adsorbed around the pillar ligand in a different manner from that at Site II, where the molecule is surrounded by three terephthalate ligands (named Site III). Totally fifteen to sixteen CO_2 molecules are adsorbed into one unit cell of UiO-66. The binding energy (BE) decreases in the order Site I > Site III > Site II for all three molecules studied here and in the order acetone > methanol >> CO_2 in the three adsorption sites. At the site I, the protonic H atom of the $\mu\text{-OH}$ group interacts strongly with the negatively charged O atom of CO_2 , acetone and methanol, which is the origin of the largest BE value at this site. Although the DFT calculations present these decreasing orders of BE values correctly, the correction by post-Hartree-Fock calculations is not negligibly small and must be added for obtaining better BE values. We explored NMR spectra of UiO-66 with adsorbed CO_2 molecules and found that the isotropic shielding constants of the ^1H atom significantly differ among no CO_2 , one CO_2 (at Sites I, II, or III), and fifteen CO_2 adsorption cases (Sites I to III) but the isotropic ^{17}O and ^{13}C shielding constants change moderately by adsorption of fifteen CO_2 molecules. Thus, ^1H NMR measurement is one of useful experiments for investigating CO_2 adsorption.

Introduction

The zirconium-based metal-organic framework (MOF) $[\text{Zr}_6\text{O}_4(\text{OH})_4(\text{bdc})_6]_n$ (bdc = benzene-1,4-dicarboxylate) was synthesized by Lillerud and coworkers and named UiO-66.¹²³⁴ In UiO-66, one OH group bridges three Zr atom and one bdc ligand bridges two Zr atoms, as shown in Scheme 1A, and there exist tetrahedral and octahedral cages (Scheme 1B). The UiO-66 and related MOFs have attracted great interest as excellent functional materials, as discussed in many review articles.⁵⁶⁷⁸⁹¹⁰¹¹¹² One of the reasons is their exceptionally high thermal and chemical stabilities compared to other MOFs. Particularly, UiO-66 and related MOFs are stable towards water atmosphere^{1,2,6,7,11,12} in contrast to other MOFs, which generally exhibit poor hydrothermal stability probably due to weak metal-linker bonds. Because of their high stability towards water, UiO-66 and related MOFs are recognized as excellent materials for wastewater treatment and water harvester.^{7,12}

Scheme 1. Structural formula of UiO-66 $[\text{Zr}_6\text{O}_4(\text{OH})_4(\text{bdc})_6]_n$ (bdc = benzene-1,4-dicarboxylate) (A) and its porous structure (B)



MOFs are believed to be useful for gas adsorption, separation, and storage because of the huge

surface area and controlled pore structure, as suggested previously¹³ and reviewed recently.¹⁴¹⁵¹⁶¹⁷¹⁸ One of the important target uses for MOFs is the capture of carbon dioxide (CO_2) molecule, as discussed in many excellent works¹⁹²⁰²¹²²²³²⁴²⁵²⁶²⁷²⁸²⁹ including reviews in the last decade.^{22,24,26} However, many MOFs possessing weak metal-linker bonds are not useful for post-combustion capture of CO_2 because the combustion gas contains water (H_2O) in almost all cases. In this regard, UiO-66 and related MOFs are promising candidates for such post-combustion CO_2 capture because of the excellent stability towards water.²⁷⁻²⁹ For developing further the chemistry of CO_2 adsorption to UiO-66 and related MOFs, we need detailed knowledge of CO_2 adsorption such as the adsorption position of CO_2 , its binding energy with MOFs, and the strength and nature of interaction between CO_2 and MOFs. In one pioneering work, Peterson and coworkers experimentally investigated CO_2 and CD_4 adsorptions into UiO-66(Zr) and theoretically analyzed those adsorptions using the infinite UiO-66 crystal model.³⁰ In their work, CO_2 and CD_4 adsorption positions were determined and the relation between the host-guest interaction and the concentration of CO_2 was discussed, whereas the dispersion interaction was considered using a DFT functional including an empirical dispersion correction but no post-Hartree-Fock correction was made. Recently, Nandy and coworkers investigated NMR chemical shifts of adsorbed acetone and methanol and theoretically analyzed the experimental observations using DFT calculations on a cluster model,³¹ where the Zr moiety was excluded from the model to save computational cost. Because it is not easy to observe experimentally correct positions of gas molecules adsorbed to MOFs due to flexible adsorption structure, computational results of CO_2 adsorption positions, binding energies, and NMR shielding constants are of great value to the chemistry of CO_2 adsorption to UiO-66.

Here, we theoretically investigated adsorption positions and adsorption energies of CO_2 , methanol, and acetone molecules using DFT calculations with post-Hartree-Fock corrections and

NMR chemical shifts of UiO-66 with adsorbed CO₂ molecules using DFT calculations. Our purposes here are to obtain computational knowledge of adsorption position and binding energy of CO₂ when UiO-66 is fully loaded with CO₂ molecules, to compare these with those of acetone and methanol, and to elucidate how much NMR shielding constants change by CO₂ adsorption. We believe that these computational results provide us with a good understanding of CO₂ adsorption to UiO-66.

Modeling and Computational Details

Peterson and coworkers experimentally and theoretically reported that sixty CO₂ molecules are adsorbed into one conventional unit cell of UiO-66;³⁴ the adsorption of sixty CO₂ molecules to one conventional unit cell corresponds to the adsorption of fifteen CO₂ molecules to one primitive unit cell. In this work, we mainly investigated the adsorption of fifteen CO₂ molecules into one primitive unit cell. In addition, we investigated the adsorption of sixteen CO₂ molecules into one primitive unit cell to make sure if the adsorption of fifteen gas molecules is the maximum; details are described below. To find the adsorption positions and orientations of CO₂ molecules, we first carried out canonical Monte-Carlo (MC) simulations using Materials Studio.³² The standard universal force field (UFF)³³ was used to describe the van der Waals interactions between a gas molecule and UiO-66 and between gas molecules. The electrostatic interaction was evaluated using the Ewald summation method with atomic charges calculated by the charge equilibration method.³⁴ First, an MC simulation of 1×10^7 steps was carried out for reaching equilibration, followed by an MC calculation of 2×10^7 steps to obtain the best adsorption position(s). The positions of the CO₂ molecules can be classified into three groups, Sites I, II, and III, as discussed in the next section. In the case of acetone and methanol, the adsorption amounts have not been reported in experiment. For comparison with CO₂ adsorption, we carried out an MC simulation of UiO-66 with fifteen

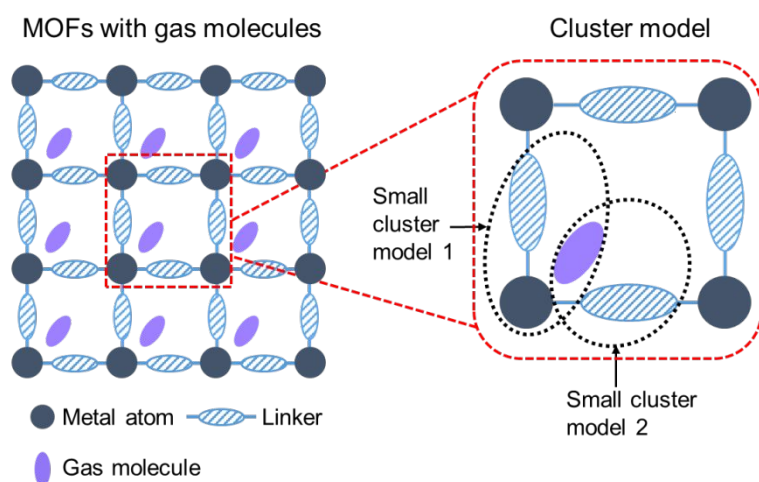
molecules of acetone and methanol, and found that fifteen molecules are adsorbed at Sites I, II, and III in a similar manner to the CO₂ case. Even though acetone and methanol are moderately larger than CO₂, a significant difference was not observed, as discussed below. These results suggest that the adsorption of fifteen molecules is realistic in the acetone and methanol cases.

Next, the adsorption positions and orientations of gas molecule(s) were optimized by DFT calculations under periodic boundary conditions, starting from the geometry obtained by the MC simulation. Because absorption of gas molecules to MOFs has been successfully investigated by means of DFT calculations using functionals including dispersion correction, as reviewed elsewhere,^{35,36} the Perdew–Burke–Ernzerhof (PBE) functional³⁷ with Grimme’s D3 dispersion correction (PBE-D3)³⁸ was used here, where plane wave basis sets were employed with the cutoff energy of 500 eV and the core–valence electron interactions were described by the projector augmented-wave (PAW) method.^{41,42} Γ –point sampling of the Brillouin zone was employed in all DFT calculations. The k -point mesh was sampled using an $1 \times 1 \times 1$ Monkhorst-Pack grid.

In the geometry optimization, the cell parameters and atomic positions were optimized until all atomic forces became smaller than 0.01 eV/Å. The Vienna Ab Initio Simulation Package (VASP 5.4.1)^{43,44} was used for the periodic DFT calculations.

To characterize each adsorption site, we calculated the adsorption energy of one gas molecule with one unit cell, where the adsorption geometry of one gas molecule was reoptimized using DFT under periodic boundary conditions. Although the DFT-calculated binding energies using dispersion correction functionals are in better agreement with experimental results,^{35,36} the dispersion interaction is more reliably calculated with post-Hartree-Fock methods such as the Møller-Plesset second-order perturbation (MP2) method, the coupled cluster singles and doubles method with perturbative triples (CCSD(T)), or similar methods, with DFT with dispersion correction functionals. For this reason, the computational method composed of the DFT calculations on an infinite system

and post-Hartree-Fock calculations on a cluster model has been used for evaluating the binding energy (BE) of gas molecule to MOF,^{45–49} where the periodic boundary condition was used for DFT calculations and a cluster model is shown in Scheme 2 as an example. This method was recently named the cluster model/periodic model (CM/PM)-combined method.⁵⁰ The CM/PM-combined method resembles the ONIOM method proposed by Morokuma and coworkers.^{51,52} But, the quality of computation here is slightly lower than with the two-layer ONIOM method, as described below.



Scheme 2. Schematic representation of periodic model and cluster model

In the CM/PM-combined method, the binding energy (BE) of gas molecule (G) with infinite UiO-66 is first evaluated using DFT with the PBE-D3 functional under periodic boundary conditions, as described by eq (1):

$$BE^{\text{PBE-D3:PBC}}(\text{INF}) = E_t^{\text{PBE-D3:PBC}}(\text{UiO-66} \cdot G) - E_t^{\text{PBE-D3:PBC}}(\text{UiO-66}) - E_t^{\text{PBE-D3:PBC}}(G)$$

(1)

where geometries of UiO-66 with gas molecule, UiO-66 and gas molecule are optimized and the superscript “PBE-D3:PBC” denotes that DFT calculation with the PBE-D3 functional was carried out under periodic boundary conditions (PBC) and in parentheses indicate calculated systems; for

instance, INF represents an infinite system consisting of UiO-66 with an adsorbed gas molecule, and G and UiO-66·G mean, respectively, gas molecule and UiO-66 adsorbed with G molecule. The gas molecule G was calculated by DFT under periodic boundary conditions, placing one G molecule in a large box ($25 \times 25 \times 25 \text{ \AA}^3$). In this work, we evaluated BE for adsorption of one gas molecule and compared it among several adsorption sites; the purpose of the BE calculation is to characterize the adsorption site. For obtaining an improved BE value, we evaluated a correction ΔE_{cor} term at the post-Hartree-Fock level, as shown by eq. (2), to calculate the dispersion interaction at a higher level of theory than DFT,

$$\Delta E_{\text{cor}}(\text{CM}) = BE^{\text{post-HF}}(\text{CM}) - BE^{\text{PBE-D3}}(\text{CM}) \quad (2)$$

where (CM) means a cluster model and the superscripts “post-HF” and “PBE-D3” represent, respectively, that the post-Hartree-Fock method and the DFT with the PBE-D3 functional were used for evaluating the BE value. In this calculation, the structures of CM and G were taken to be the same as those in the optimized geometry of the infinite UiO-66 with adsorbed G molecule, where the dangling bonds of the cluster model were capped with hydrogen atoms; this $\Delta E_{\text{cor}}(\text{CM})$ corresponds to the difference in the BE value between the DFT and post-Hartree-Fock calculations using a cluster model. For selecting an appropriate post-Hartree-Fock method, we compared the interaction energy of G calculated with cluster model between spin-component scaled MP2 theory (SCS-MP2)⁵⁴ and the MP2.5 method,⁵⁵ where the interaction energy is defined as an energy difference between the cluster model with gas molecule and the sum of the isolated cluster model and gas molecule; note their geometries were not optimized but taken to be the same as those in the total system. As shown in Table S1 of the Supporting Information, that the MP2.5-calculated value is closer to the CCSD(T) value than the SCS-MP2 value. However, the MP2.5 calculation has a considerably larger computational cost than the SCS-MP2 calculation because the MP3 calculation is more expensive than the MP2 calculation. The cluster model employed in this work is not small,

as described in the next section. Therefore, we further divided CM into several small cluster models, named SCM-*i*, as shown in Scheme 1, and calculated the $\Delta E(\text{CM})_{\text{cor}}$ value using the SCS-MP2 method for the CM cluster model and the MP2.5 method for the smaller cluster models SCM-*i*, as shown by eq. (3);

$$\Delta E_{\text{cor}}(\text{CM}) = BE^{\text{SCS-MP2}}(\text{CM}) - BE^{\text{PBE-D3}}(\text{CM}) + \sum_i [BE^{\text{MP2.5}}(\text{SCM} - i) - BE^{\text{SCS-MP2}}(\text{SCM} - i)] \quad (3)$$

where the geometries of SCM-*i* and G are taken to be the same as those in the optimized geometry of infinite UiO-66 with adsorbed G molecule. The second term of the right-hand side of eq. (3) indicates that the additional correction at the MP2.5 level is made using several smaller cluster models; see Scheme 1 for its example. Because of the use of smaller cluster models in addition to a cluster model, the quality of this CM/PM-combined method is a bit lower than that of the two-layer ONIOM method, as mentioned above. However, this type of correction with smaller cluster models provides reliable binding energy when the correction is made for the dispersion interaction of the van der Waals adduct.⁵⁶ The finally obtained $BE^{\text{CM/PM}}$ value is represented by eq. (4).

$$BE^{\text{CM/PM}} = BE^{\text{PBE-D3:PBC}}(\text{INF}) + \Delta E_{\text{cor}}(\text{CM}) \quad (4)$$

In the SCS-MP2 and MP2.5 calculations, the augmented correlation-consistent polarized valence double-zeta (aug-cc-pvdz) basis sets were used for all atoms except Zr, for which the Stuttgart-Dresden-Bonn basis set was used with corresponding effective core potentials.⁵⁷ The basis set superposition error (BSSE) was removed using the counterpoise method.⁵⁸ These post-Hartree-Fock calculations were carried out using Gaussian16 program.⁵⁹

Nuclear shielding tensors were calculated using the DFT method with the PBE-D3 functional under periodic boundary conditions, where the cut-off energy of the plane wave basis sets was increased to 850 eV to improve the quality of the basis sets. For this calculation, the VASP program^{43,44} was used.

Results and discussion

Adsorption positions of carbon dioxide (CO₂), acetone, and methanol: First, we carried out classical MC simulations using the primitive unit cell shown in Figure 1, to explore whether or not fifteen CO₂ molecules can be adsorbed to UiO-66 in a reasonable manner, which moiety of UiO-66 is effective for CO₂ adsorption, and what orientation CO₂ molecules have. Starting from the obtained geometry, the geometry of UiO-66 with fifteen adsorbed CO₂ molecules was further refined by optimization with the DFT calculations under periodic boundary conditions. As shown in Figure 1(a), fifteen CO₂ molecules can be accommodated in one unit cell in a reasonable manner. The positions and orientations of these CO₂ molecules follow the R3 symmetry (Figure 1(b)). Three CO₂ molecules (blue) interact with three μ_3 -OH groups bridging three Zr atoms; details are discussed below. This adsorption site is named Site I. Although each unit cell has four μ_3 -HO-Zr₃ groups that construct a tetrahedra-like structure, three CO₂ molecules were adsorbed at three of those μ_3 -HO-Zr₃ groups but the fourth μ_3 -HO-Zr₃ group does not undergo CO₂ adsorption: the adsorption of all four sites is discussed below.

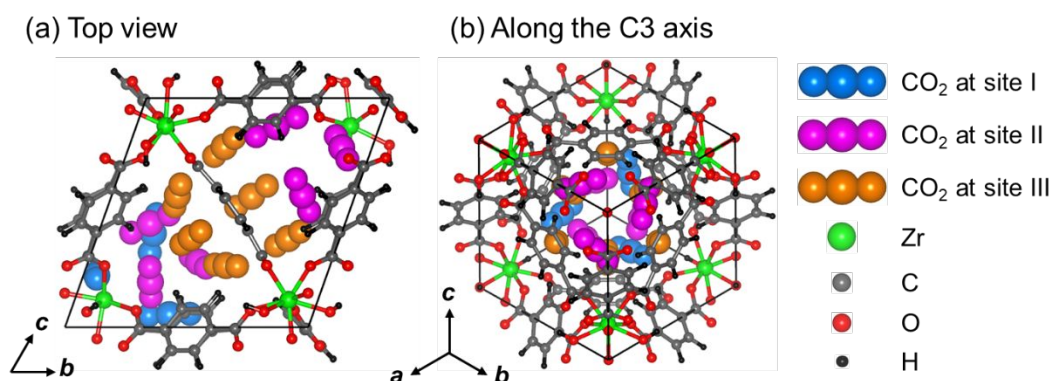


Figure 1. (a) Top view of the optimized structure for CO₂ adsorption into UiO-66, where 15 CO₂ molecules were adsorbed at three different sites, and (b) side-view along the C₃ axis.

Six CO₂ molecules (brown) are found at positions different from Site I (Figure 1(a)); this adsorption site (named Site II) is close to the terephthalate ligand. The remaining six CO₂ molecules (purple) are found at different positions (named Site III) from Sites I and II. This Site III is close to the terephthalate ligand, too. Although six CO₂ molecules are located at each of the Sites II and III in Figure 1(b), only three of them are visible in Figure 1(b) with remaining three CO₂ molecules being hidden behind the three visible CO₂ molecules (purple and brown) at each adsorption Site II or III.

Because the CO₂ adsorption at the fourth μ_3 -HO-Zr₃ site was found not to occur by the MC simulation, we further carried out MC simulation using sixteen CO₂ molecules to investigate whether the fourth μ_3 -HO-Zr₃ site undergoes CO₂ adsorption or not. The MC simulation showed that the sixteenth CO₂ molecule was not adsorbed at this site but it was found at a new site (Figure S1 of the Supporting Information). The geometry optimization was further carried out using DFT under the periodic boundary conditions. In the new site, the CO₂ molecule is slightly more distant from the terephthalate ligand than at Sites II and III; it is surrounded by three CO₂ molecules at Site III.

We were concerned that the MC simulation did not show all possible CO₂ adsorptions because of insufficient simulation time. Therefore, we placed the sixteenth CO₂ molecule at the Site I near the fourth μ_3 -HO-Zr₃ site and performed the geometry optimization with DFT under periodic boundary conditions. This CO₂ molecule is bound well at the μ_3 -HO-Zr₃ site; see Figure S1(B). The binding energy $BE^{\text{PBE-D3:PBC}}(\text{INF})$ at Site I (−11.51 kcal/mol) is larger in magnitude than that (−9.38 kcal/mol) at the new site.⁶⁰ These results strongly suggest that four CO₂ molecules are adsorbed at four Site I in one primitive unit cell and totally sixteen CO₂ molecules are adsorbed into one primitive unit cell. It is an important issue how many CO₂ molecules can be adsorbed

into UiO-66 and a further careful study is needed. However, we focus here on the adsorption of fifteen CO₂ molecules according to the previous study,³⁰ because the sixteenth CO₂ adsorption influences little the other CO₂ adsorption at Site I, as shown in Figure S1, and the adsorption structure obtained for one CO₂ molecule at each adsorption site was employed for characterization of each adsorption site after re-optimization of the adsorption structure.

At Site I, three CO₂ molecules are bound with three μ_3 -HO-Zr₃ groups; one of them is shown by the cluster model **C I** and the small cluster model **C Ia** in Figure 2(a). This adsorption site corresponds to the TcOH site in the previous report.³⁰ The optimized distance (2.172 Å) between the O atom of CO₂ and the H atom of the μ_3 -OH is shorter than the experimental value (2.40 Å)³⁰ but agrees with the previously optimized value (2.19 Å) by DFT calculation when fifteen CO₂ molecules are adsorbed to one unit cell.^{30,61} This distance is much shorter than the O--H distance (3.503 Å to 3.582 Å) between the oxygen atom of CO₂ and the hydrogen atom of the terephthalate

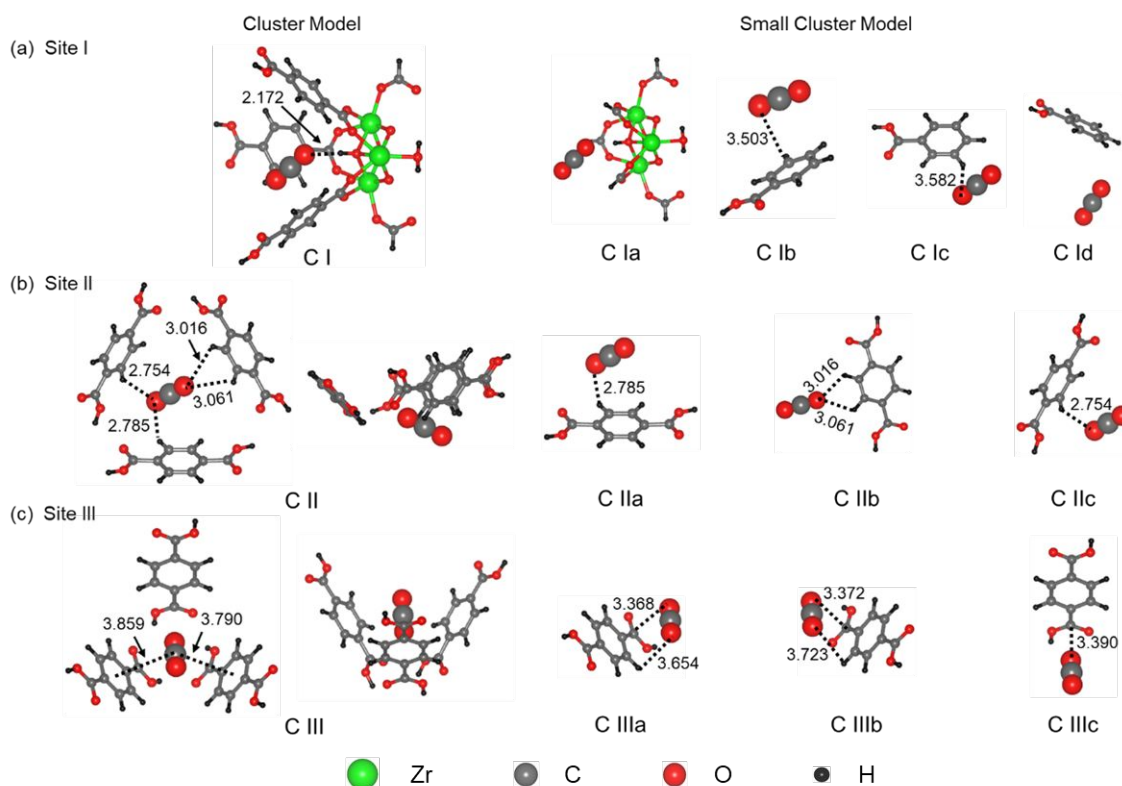


Figure 2. Cluster models and small cluster models of CO₂ adsorption at Sites I, II, and III, where the terephthalate linkers are modeled by terephthalic acids. The numbers in the figure represent distances in angstrom.

ligand (**C Ib** and **C Ic** in Figure 2(a)), the reason for which is discussed below. The CO₂ molecule is parallel to one C₆H₄ ring of terephthalate ligand (**C Ib** in Figure 2(a)) to form an attractive π - π interaction with the C₆H₄ ring. However, the interactions with the other C₆H₄ rings seem weak because of the long distance (**C Ic** in Figure 2(a)) and unfavorable orientation (**C Id** in Figure 2(a)). These features suggest that the interaction between the CO₂ and the terephthalate ligands is weak in Site I.

At Site II, the top view shows that the adsorbed CO₂ molecule is surrounded by three C₆H₄ rings of terephthalate ligands but only loosely so, as shown by **C II** of Figure 2(b). This adsorption site corresponds to the Ow site (window between two octahedral cages) previously defined.³⁰ The negatively charged oxygen atom of the CO₂ approaches two positively charged hydrogen atoms of the two C₆H₄ rings; the distances are 2.785 ~ 2.754 Å (**C IIa** and **C IIc**). This electrostatic interaction is not strong because the atomic charge of the hydrogen atom is moderate. The oxygen atom of the CO₂ is very distant from the hydrogen atoms of the remaining C₆H₄ ring (**C IIb**) and the CO₂ molecule is not parallel with the C₆H₄ rings, suggesting that the π - π interaction is weak. Overall, the interaction between CO₂ and the three terephthalate ligands is weak at Site II.

At Site III, each CO₂ molecule is surrounded by three C₆H₄ planes of terephthalate ligands; see **C III** in Figure 2(c). The top view and side view of **C III** show that the CO₂ molecule is parallel to two C₆H₄ planes, with rather long distances between the carbon atom of the CO₂ and the center of these two C₆H₄ planes of 3.790 Å and 3.859 Å. However, the CO₂ is almost perpendicular to the remaining C₆H₄ ring. This adsorption site corresponds to Wt site (window between tetrahedral and octahedral cages)

previously found;³⁰ Figure S2 in the Supporting Information shows more clearly this structure from a different direction. The smaller cluster models **C IIIa** and **C IIIb** show that one negatively charged oxygen atom of CO₂ resides above the positively charged carboxyl carbon atom and the other oxygen atom resides above the positively charged hydrogen atom. Despite the long C--O distance (3.388 Å and 3.372 Å in **C IIIa** and **C IIIb**, respectively) and the long O--H distance (3.654 Å and 3.723 Å in **C IIIa** and **C IIIb**, respectively), these structural features induce an attractive electrostatic interaction between the CO₂ and the terephthalate ligands, recalling that CO₂ is non-polar but has a quadrupole moment. The cluster model **C IIIc** indicates that the oxygen atom of the CO₂ approaches the carboxyl carbon atom in an almost perpendicular manner to the remaining C₆H₄ ring, contributing to the electrostatic interaction because the carboxyl carbon atom is positively charged and the quadrupole moment of CO₂ contributes to the electrostatic interaction with the positively charged carbon atom. These geometrical features suggest that the CO₂ adsorption occurs more strongly at Site III than at Site II, as discussed below.

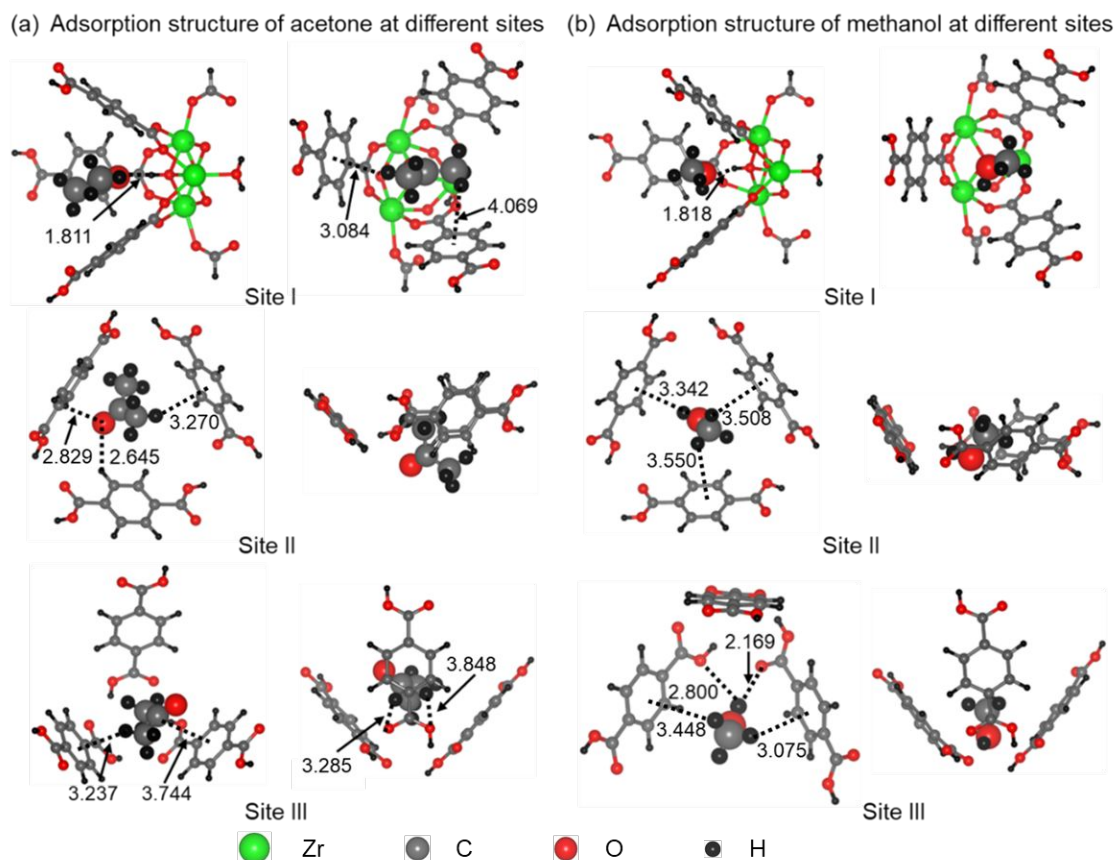


Figure 3. Adsorption structures of acetone (a) and methanol (b) into UiO-66 at sites I, II, and III. Bond distances in angstrom.

We optimized the adsorption structures of acetone and methanol in a similar way. As for CO_2 , three adsorption sites are found for both acetone and methanol; see Figure 3. At Site I, the O--H distance between the oxygen atom of acetone/methanol and the hydrogen atom of the μ_3 -OH group (1.811 Å and 1.818 Å, respectively) is considerably shorter than for CO_2 (2.172 Å). These shorter distances result from the stronger Lewis basicity of the oxygen atom in acetone and methanol than in CO_2 ; since the μ_3 -OH moiety is a Brønsted acid, the interaction between the oxygen atom of these three gas molecules and the μ_3 -OH group depends on the basicity of the gas molecule. The oxygen atomic charge gets more negative in the order CO_2 ($-0.21 e$) \ll methanol ($-0.64 e$) $<$ acetone ($-0.77 e$), suggesting that the Lewis basicity increases in this order. An additional factor is the polarity of the gas

molecule; acetone and methanol are polar but CO_2 is non-polar. Having a stronger Lewis basicity and a larger polarity than CO_2 , acetone and methanol can form a stronger electrostatic attraction with the polar $\text{Zr}-\mu\text{-OH}$ moiety than does CO_2 and approach more closely the HO-Zr moiety to induce the larger binding energies than does CO_2 , as discussed in the next section.

At Site II, the oxygen atom of acetone interacts with one hydrogen atom of terephthalate ligands and with the positively charged carboxyl carbon atom, and one C-H bond of one methyl group approaches the C_6H_4 ring to form a $\text{CH}-\pi$ interaction, as shown by the middle structure in Figure 3(a). On the other hand, methanol does not form a similar electrostatic interaction between the hydrogen atom of terephthalate ligand and the oxygen atom of methanol, as shown by the middle structure in Figure 3(b). Instead, methanol forms one $\text{OH}-\pi$ interaction between its OH group and one C_6H_4 ring and two $\text{CH}-\pi$ interactions between the CH bonds of the methyl group and the C_6H_4 ring; however, these $\text{CH}-\pi$ interactions are weak because of a longer distance and unfavorable orientation.

At Site III, two methyl groups of acetone form two $\text{CH}-\pi$ interactions with the C_6H_4 rings of the ligands, one strong and one weak (Figure 3a; bottom). Its oxygen atom interacts with two CH bonds of two C_6H_4 rings, one strongly and one weakly. The CH bonds of methyl group forms one strong $\text{CH}-\pi$ and one weak $\text{CH}-\pi$ interactions. In the case of methanol, the oxygen atom does not form any electrostatic interaction with the hydrogen atom of the terephthalate ligand but the protonic hydrogen atom of the methanol OH group forms one strong and one weak hydrogen-bonding-like interactions with two oxygen atoms of the carboxyl group of the ligand (Figure 3b, bottom). The methyl group also approaches the C_6H_4 rings to form one strong $\text{CH}-\pi$ and one weak $\text{CH}-\pi$ interactions. All these intermolecular interactions seem reasonable.

Adsorption energies of CO_2 , acetone, and methanol molecules: In the chemistry of gas adsorption

to MOF, the adsorption energy is an important property but its correct evaluation is difficult for several reasons: (i) the dispersion interaction is important particularly when MOF has no open metal site; (ii) the electrostatic interaction is important for polar molecules because the infinitely periodic structure of MOF may strengthen or weaken it at a given position. In the case of UiO-66, both factors must be taken into consideration because UiO-66 does not have an open metal site and also has highly polarized Zr-O coordination bonds. Although CO₂ is a non-polar molecule, its adsorption energy would depend on electrostatic potential of MOF because CO₂ has negatively charged oxygen atoms, a positively charged carbon atom, and quadrupole moment. Hence, both the periodic structure of UiO-66 and the dispersion interaction must be evaluated correctly. It is likely that the electrostatic interaction can be reliably described by DFT. For the dispersion interaction, however, post-Hartree-Fock methods such as the MP2, SCS-MP2, and CCSD(T) are more reliable than DFT. Here, we employed the CM/PM-combined method consisting of DFT calculations of the infinite structure of UiO-66 under periodic-boundary conditions and SCS-MP2 and MP2.5 calculations of cluster models, as described in the section of Modeling and Computational Details. To characterize three adsorption sites, we evaluated the adsorption energy of one gas molecule here.

CO₂ at Site I: At Site I, CO₂ molecule approaches the bridging μ_3 -OH ligand coordinating with three Zr atoms. Since the Zr-O coordination bond considerably influences the protonic character of the hydrogen atom, we included the Zr moiety in the cluster model **C I**; see Figure 2(a). As discussed in the Computational Section, we calculated the *BE* value using the MP2.5 method since it reproduces the CCSD(T)-calculated interaction energy between CO₂ and the ligand moiety better than does the SCS-MP2 method. However, because of the MP2 component, the MP2.5 calculation is too expensive for the cluster model **C I**. We therefore divided the cluster model **C I** into several smaller models, **C Ia**, **C Ib**, **C Ic**, and **C Id** (Figure 2(a)). We likewise divided the cluster models **C II** and **C III** into smaller cluster models (Figure 2(b) and (c)). The $BE^{\text{PBE-D3}}(\text{INF})$ value obtained by eq. (1) is -7.68 kcal/mol (a negative

value means stabilization energy), which is the largest among the three adsorption sites, as shown in Table 1. The PBE-D3-calculated $BE^{\text{PBE-D3}}(\text{CM})$ value of the cluster model **C I** is more negative than the corresponding SCS-MP2-calculated $BE^{\text{SCS-MP2}}(\text{CM})$ value by 1.19 kcal/mol, suggesting that the PBE-D3 method overestimates the adsorption energy and a post-Hartree-Fock correction is needed for evaluating correctly the BE value.

Table 1. DFT-calculated binding energy ($BE^{\text{PBE-D3:PBC}}(\text{INF})$) of infinite system, SCS-MP2- and PBE-D3-calculated binding energies ($BE^{\text{SCS-MP2}}(\text{CM})$ and $BE^{\text{PBE-D3}}(\text{CM})$) using cluster model (**C I**, **C II**, or **C III**), correction term of BE value by MP2.5 calculations using small cluster models $\Delta E_{\text{cor}}^{\text{MP2.5-SCS-MP2}}(\text{SCM})$, and $BE^{\text{CM/PM}}$ calculated by the CM/PM-combined method (in kcal/mol)

	Infinite System	Cluster Model (CM)		Small Cluster model (SCM)	CM/PM-combined method
	$BE^{\text{PBE-D3:PBC}}(\text{INF})$	$BE^{\text{PBE-D3}}(\text{CM})$	$BE^{\text{SCS-MP2}}(\text{CM})$	$\Delta E_{\text{cor}}^{\text{MP2.5-SCS-MP2}}(\text{SCM})^a$	$BE^{\text{CM/PM}}$
CO ₂					
Site I	-7.68	-7.04 (with C Ia) -5.08 (without C Ia)	-5.85 (with C Ia) -3.88 (without C Ia)	-0.92 (with C Ia) -0.52 (without C Ia)	-7.41 (with C Ia) -7.00 (without C Ia)
Site II	-4.19	-3.55	-1.87	-0.48	-2.99
Site III	-6.19	-5.41	-4.25	-0.47	-5.50
Acetone					
Site I	-18.70	-9.77	-7.60	-1.45	-17.99
Site II	-10.99	-9.17	-5.81	-1.41	-9.03
Site III	-12.50	-8.44	-5.97	-1.09	-11.11
Methanol					
Site I	-14.71	-6.53	-4.24	-1.25	-13.67
Site II	-8.80	-7.03	-4.50	-0.91	-7.18
Site III	-9.52	-8.17	-4.93	-1.34	-7.62

^a $\Delta E_{\text{cor}}^{\text{MP2.5-SCS-MP2}}(\text{SCM}) = \sum_i [BE^{\text{MP2.5}}(\text{SCM} - i) - BE^{\text{SCS-MP2}}(\text{SCM} - i)]$;
 $BE^{\text{MP2.5}}(\text{SCM} - i)$ and $BE^{\text{SCS-MP2}}(\text{SCM} - i)$ values are presented in Table S2 of the Supporting Information.

We then evaluated the correction term $\Delta E_{cor}^{MP2.5-SCS-MP2}$ (SCM) using small cluster models **C Ia**, **C Ib**, **C Ic**, and **C Id**. This term is about 1 kcal/mol, indicating that the SCS-MP2 method tends to underestimate BE values and that the MP2.5 correction must be added to recover the underestimated $BE^{SCS-MP2}$ (SCM) value to some extent. A similar result, the underestimation of BE by the MP2 method and its partial recovery by the CCSD(T) method, was reported in a theoretical work of CO₂ adsorption to MOF.⁵¹ In addition, we calculated the post-Hartree-Fock correction without the small cluster model **C Ia** which contains the μ_3 -HO-Zr moiety (Figure 2(a)). The BE^{PBE-D3} (CM) value without **C Ia** is considerably smaller than the BE^{PBE-D3} (CM) value with **C Ia** by 1.19 kcal/mol, showing that the Zr moiety must be contained in the cluster model to obtain a reliable BE energy. However, the $BE^{SCS-MP2}$ (CM) value of the cluster model without **C Ia** is also considerably smaller than the BE^{PBE-D3} (CM) value with **C Ia** by 2.0 kcal/mol. The $\Delta BE^{MP2.5-SCS-MP2}$ (SCM) value obtained for the small cluster models **C Ib**, **C Ic**, and **C Id** without **C Ia** is also smaller by 0.4 kcal/mol than that obtained for all the small cluster models, **C Ia**, **C Ib**, **C Ic**, and **C Id**. The total correction ($-1.19 - (-2.0) - 0.40$) kcal/mol) is -0.41 kcal/mol. As a result, the $BE^{CM/PM}$ value is -7.41 kcal/mol when **C Ia** is included and 7.00 kcal/mol when **C Ia** is excluded, indicating that the post-Hartree-Fock correction is about 3.5% of $BE^{PBE-D3:PBC}$ (INF) when **C Ia** is involved and 8.9% of $BE^{PBE-D3:PBC}$ (INF) when **C Ia** is not. These results imply that the interaction with the μ_3 -HO-Zr₃ moiety is important for obtaining the BE value of CO₂ with UiO-66 but that the post-Hartree-Fock correction is not very large for this **C Ia** (about 5 % of $BE^{PBE-D3:PBC}$ (INF)). This is reasonable because the electrostatic interaction between the negatively charged oxygen atom of CO₂ and the positively charged hydrogen atom of the μ_3 -HO-Zr₃ moiety contributes largely to the BE (CM) and it can be evaluated well at the DFT level. Therefore, the post-Hartree-Fock correction of **C Ia** is not important at Site I compared to other Sites II and III.

CO₂ at Site II: At Site II, one oxygen atom of CO₂ interacts with two C-H bonds of two C₆H₄ rings of the terephthalate ligands and the remaining oxygen atom interacts with two C-H bonds of one

C₆H₄ ring (**C IIa** and **C IIc** in Figure 2). Although the electrostatic interaction plays an important role in such a case, it is likely that the dispersion interaction is also important because the π -electron system of CO₂ approaches the π -electron system of the C₆H₄ moieties (see **C IIa** and **C IIc** in Figure 2(b)). This is the reason why we employed the post-Hartree-Fock calculations using cluster models in this work. We found two important results, as follows.

The first one is the somewhat large difference between $BE^{\text{PBE-D3:PBC}}(\text{INF})$ and $BE^{\text{PBE-D3:PBC}}(\text{CM})$, where CM is a cluster model of Site II shown in Figure 2(b); the $BE^{\text{PBE-D3:PBC}}(\text{CM})$ is about 15 % smaller than the $BE^{\text{PBE-D3:PBC}}(\text{INF})$. This result shows that the use of a cluster model is not good for obtaining a reliable BE value. The other is the considerably large difference between the $BE^{\text{PBE-D3}}(\text{CM})$ and $BE^{\text{SCF-MP2}}(\text{CM})$ values (Table 1), suggesting that the dispersion interaction must be evaluated at the post-Hartree-Fock level. As a result, the BE value decreases by 1.68 kcal/mol (−1.87 kcal/mol – (−3.53 kcal/mol)) by the SCS-MP2 correction. The $\Delta BE^{\text{MP2.5-SCS-MP2}}(\text{SCM})$ term partially recovers this value by 0.48 kcal/mol. The final $BE^{\text{CM/PM}}$ value with all corrections is considerably smaller than the $BE^{\text{PBE-D3:PBC}}(\text{INF})$ value by 1.20 kcal/mol (Table 1). The post-Hartree-Fock correction is considerably large, about 28.6 % of the $BE^{\text{PBE-D3:PBC}}(\text{INF})$ value.

CO₂ at Site III: At Site III, the $BE^{\text{PBE-D3:PBC}}(\text{INF})$ value is larger than that of Site II but smaller than that of Site I (Table 1). The $BE^{\text{PBE-D3}}(\text{CM})$ value for the cluster model **C III** is larger than the $BE^{\text{SCS-MP2}}(\text{CM})$ value as in Site II, whereas the difference between these two values is considerably smaller than in Site II; for instance, the $BE^{\text{SCS-MP2}}(\text{CM})$ value is about 50% of the $BE^{\text{PBE-D3}}(\text{CM})$ value for Site II but about 80 % for Site III. The $\Delta BE^{\text{MP2.5-SCS-MP2}}(\text{SCM})$ value (−0.47 kcal/mol), the sum of correction terms for the small cluster models **C IIIa**, **C IIIb**, and **C IIIc** is similar to that of Site II. As a result, the BE value is recovered by 0.47 kcal/mol and the final $BE^{\text{CM/PM}}$ value (−5.50 kcal/mol) is somewhat smaller than the $BE^{\text{PBE-D3:PBC}}(\text{INF})$ value by 0.69 kcal/mol. The post-Hartree-Fock correction is about 11.1 % of the $BE^{\text{PBE-D3:PBC}}(\text{INF})$ value. Although the post-Hartree-Fock correction is significant, it is much smaller

than at Site II. This is reasonable because the electrostatic attraction is larger in the two small cluster models (**C IIIa** and **C IIIb**) at Site III than at Site II, in which an electrostatic attraction is found only in **C IIb**: In other words, the electrostatic interaction contributes more to the adsorption energy at Site III than at the Site II.

Here, we make comparison between the experimentally reported isosteric heat of the first CO₂ adsorption and the calculated binding energy of the first CO₂ adsorption at Site I because it is likely that the first CO₂ molecule is adsorbed at Site I due to the largest binding energy; note that the comparison with other experimental values is difficult because of the lack of information about the number of adsorbed CO₂ molecules at Sites I, II, and III. The calculated $BE^{CP/PM}$ value for the first CO₂ adsorption is 7.41 kcal/mol (= 31.0 kJ/mol) with the SCS-MP2 and MP2.5 corrections of **C Ia** and 7.01 kcal/mol (=29.3 kJ/mol) without the corrections of **C Ia**. The calculated values are moderately larger than the experimental values,^{62, 63, 64} similar to the previously calculated value (29.9 kJ/mol) by Zhou *et al.*,⁶⁵ but moderately smaller than the calculated value (33.3 kJ/mol) by Peterson *et al.*³⁰ Though the difference between the calculated value and the experimental one is not bad considering the large size, flexible adsorption position, and contribution of many weak interactions, further theoretical efforts are needed for better estimation of the binding energy.

Acetone and methanol at Sites I, II, and III: We evaluated the adsorption energies of acetone and methanol in a similar way to that of CO₂, whose cluster models and smaller cluster models are shown in Figures S3 and S4 of the Supporting Information. In these gas molecules, we did not include the μ_3 -HO-Zr₃ moiety in the cluster models because the post-Hartree-Fock correction is not important for the interaction with the μ_3 -HO-Zr₃ moiety in the CO₂ case; this is reasonable because the electrostatic interaction largely contributes to the BE value at Site I and the DFT method is likely to describe well the electrostatic interaction. In both acetone and methanol, the largest $BE^{CM/PM}$ value is obtained at Site I as for CO₂; see Table 1. These results clearly show that Site I is the most important adsorption site in UiO-

66 and that the μ_3 -OH group plays an important role in gas adsorption. Consistent with the large $BE^{\text{PBE-D3:PBC}}(\text{INF})$ and $BE^{\text{CP/PM}}$ values for Site I, the O--H distance is rather short (1.811 Å and 1.818 Å, respectively, as discussed above and shown in Figure 3). The $BE^{\text{CM/PM}}$ value decreases in the order Site I > Site III > Site II, as for the CO_2 case.

Summary of BE values of all gas molecules at all Sites: First, we compare here the binding energy between the post-Hartree-Fock corrected $BE^{\text{CM/PM}}$ value and the DFT-calculated $BE^{\text{PBE-D3:PBC}}$, as shown in Figure 4. Apparently, all $BE^{\text{CM/PM}}$ values are less negative than the $BE^{\text{PBE-D3:PBC}}$ values, indicating that the post-Hartree-Fock corrections decrease the binding energy; see also Table 1. However, it is noted that all $BE^{\text{CM/PM}}$ values are, to a good approximation, directly proportional to the $BE^{\text{PBE-D3:PBC}}$ values, indicating that the DFT-calculated binding energy under periodic boundary conditions is useful for semi-quantitative discussion of the binding energy.

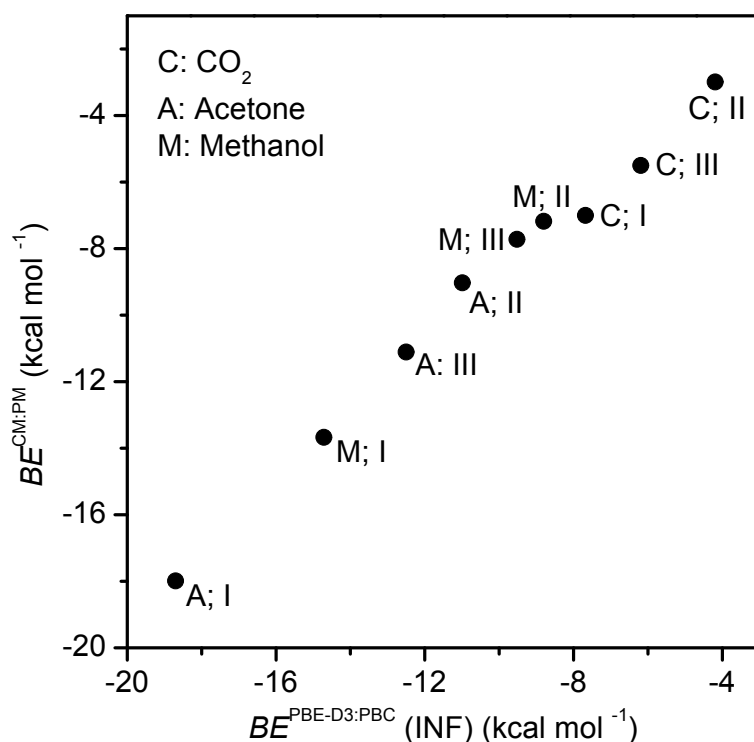


Figure 4. Comparison between $BE^{\text{CM/PM}}$ and $BE^{\text{PBE-D3:PBC}}(\text{INF})$ values for CO_2 , acetone, and methanol.

Next, we compare the binding energy at Sites I, II, and III, and for CO₂, acetone, and methanol. The $BE^{CM/PM}$ values at Sites I, II, and III decrease in the order acetone > methanol > CO₂. At Site I, this decreasing order of the binding energy is consistent with the calculated O--H distances discussed above and with our expectation based on the polarity and the negative charge of the oxygen atom of the gas molecule, as discussed above. For all three molecules, the $BE^{CM/PM}$ value decreases in the order Site I > Site III > Site II. This decreasing order can be understood in the following manner: In Site I, the negatively charged oxygen atom of the gas molecule forms a Brönsted-acid–Lewis-base interaction with the protonic hydrogen atom of the μ -OH group. It is likely that this is stronger than the CH- π , OH- π , and CH-O interactions as it represents the acid-base interaction between the protonic hydrogen atom of the μ -OH group and the negatively charged oxygen atom of gas molecule: Indeed, the decreasing order of the $BE^{CP/MP}$ value at Site I is parallel to the decreasing order of the negative charge of the oxygen atom of gas molecule (discussed above). In addition, CO₂ forms one π - π interaction with one C₆H₄ ring, and both acetone and methanol form CH- π interaction between one CH bond of their methyl groups and the C₆H₄ ring (Figure 3a). These interactions also contribute to the binding energy but they are weaker than the acid-base interaction.

At Sites II and III, these three gas molecules form typical intermolecular interactions such as CH- π , OH- π , and CH-O interactions. Although the comparison of those weak intermolecular interactions is difficult, Site III seems better than Site II because the number of intermolecular interactions is larger in Site III than in Site II; in other words, these gas molecules have better orientation and position in Site III for intermolecular interactions than in Site II.

Here, we have two important conclusions; (i) The post-Hartree-Fock correction always decreases the binding energy calculated by DFT under periodic boundary conditions. However, the DFT-calculated binding energy $BE^{PBE-D3:PBC}$ is useful for semi-quantitative discussion. And, (ii) UiO-66 is useful for

adsorption of gas molecules with Lewis base character because of the presence of the μ -OH group. If its protonic H atom is removed, the anionic μ -O group appears, which is useful for interacting with the Lewis acid and metal cation. Indeed, one experimental work recently succeeded in incorporating Cu(II) ions on the O group in UiO-66 and enhancing the adsorption of NH_3 molecules.⁶⁶

NMR Shielding Tensors: Here, we focus on the changes in NMR shielding constants by CO_2 adsorption, bearing in mind that the CO_2 adsorption to MOFs is a promising CO_2 capture technique and that NMR measurement is expected to be useful for investigating CO_2 adsorption.^{32,67,68} In Figure 5, the isotropic shielding constants $\sigma_{\text{iso}} = (\sigma_{11} + \sigma_{22} + \sigma_{33})/3$ are plotted for different numbers of adsorbed CO_2 molecules; details of the NMR shielding tensors are presented in Table S3 of the Supporting Information. We show violin plots as a visual support in Figure 4, because distributions are not unimodal and therefore poorly summarized by simple statistics such as mean values and standard deviations. In this work, we evaluated NMR shielding constants but not the corresponding NMR chemical shifts relative to the reference materials for following reasons: (1) the calculation of liquid water, which is the reference of ^{17}O chemical shift, is not easy and the value is always qualitative, and (2) the changes in NMR chemical shifts by CO_2 adsorption can be discussed well using relative values to the chemical shifts of UiO-66 without CO_2 adsorption. Here, we mainly discuss whether the NMR chemical shifts change upon the CO_2 adsorption into UiO-66 or not and how much they change.

(a) H atom shielding constants

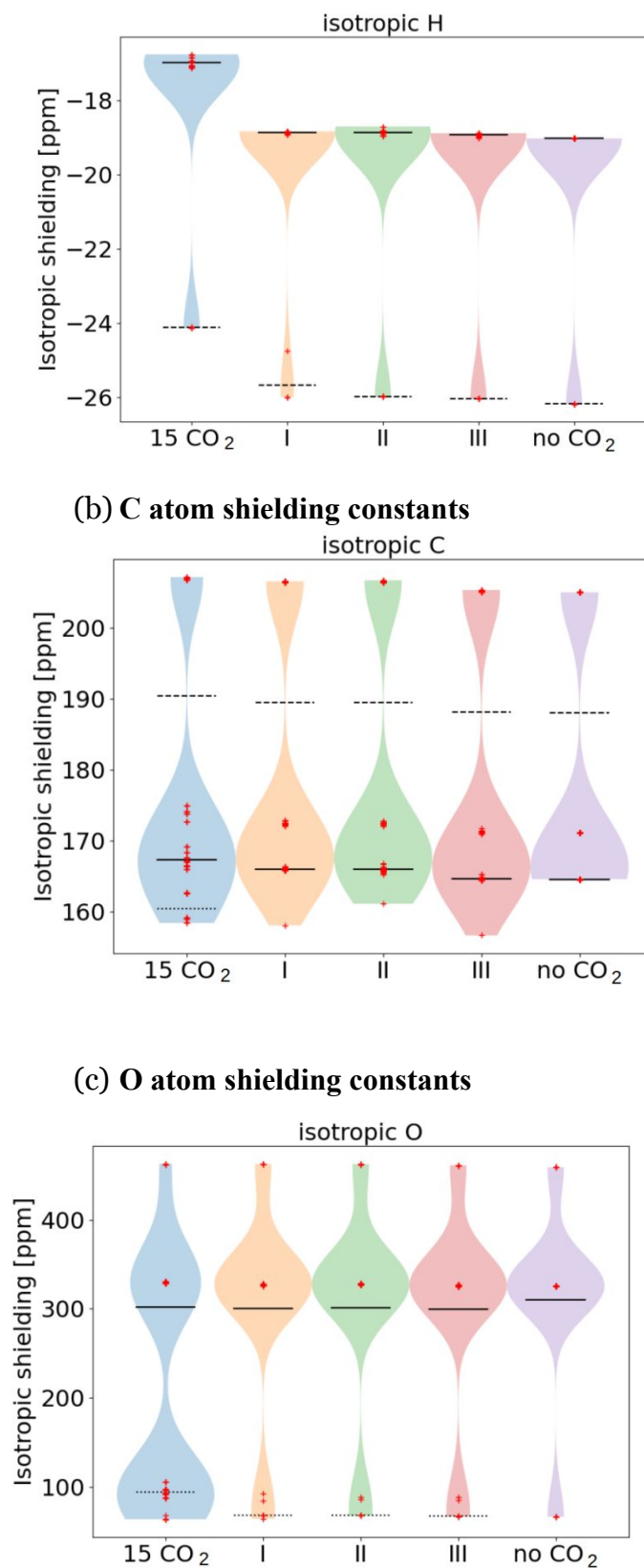


Figure 5: The calculated nuclear shielding constants of hydrogen atom^a (a), carbon atom^b (b), and oxygen atom^c (c) in UiO-66 with adsorbed CO₂. From left to right in each

subplot, the shielding constants with 15 adsorbed CO₂, 1 CO₂ at Site I, 1 CO₂ at Site II, 1 CO₂ at Site III, and no CO₂, respectively, are shown. Data points are shown as crosses. ^a Solid line and dashed line represent respectively mean values of hydrogen atoms bound to a carbon atom and all other hydrogen atoms. ^b Solid line, dashed line, and dotted line represent respectively mean values of carbon atoms bound to a hydrogen atom and all carbon atoms except that of CO₂. ^c Solid line and dotted line represent respectively mean values of all oxygen atoms except CO₂ and oxygen atoms of adsorbed CO₂ molecule.

Proton shielding constants: The hydrogen atoms of UiO-66 without CO₂ adsorption exhibit bimodal NMR shielding constants with twenty symmetrically equivalent hydrogen atoms around -19 to -20 ppm and four symmetrically equivalent hydrogen atoms at -26 ppm; see the violin plot at “no CO₂” column on the right-end of Figure 5(a). These values slightly shift upward by adsorption of one CO₂ molecule at Sites I, II, and III; see “I”, “II”, and “III” columns presented on middle in Figure 5(a). Upon CO₂ adsorption, the symmetrical equivalence disappears and the signal at -19 ppm becomes a cluster composed of several lines nearby to each other. However, the violin plot and the mean values do not significantly change, where the mean value of hydrogen atoms bound to the carbon atoms and that of the other hydrogen atoms are presented respectively by a solid and dashed lines in Figure 5(a). When fifteen CO₂ molecules are adsorbed, the NMR shielding constants of the hydrogen atoms substantially shift upward; see the violin plot at “15 CO₂” column on the left-end in Figure 5(a). In addition, the cluster of shielding constants at the upper (less negative) end broadens more than it does upon adsorption of one CO₂ molecule, suggesting that the geometry deformation occurs more by adsorption of fifteen CO₂ molecules than that by one CO₂ molecule. As a result, the violin plot and the mean value of oxygen atoms of CO₂ change somewhat.

All these computational results strongly suggest that proton NMR measurements can provide us with valuable information in studying CO₂ adsorption to UiO-66 when the CO₂ adsorption fully occurs.

Carbon shielding constants: Without CO₂ adsorption, the carbon atoms of UiO-66 exhibit non-unimodal shielding constants at three sites in the same way as for the hydrogen atoms, 165 ppm (twenty-

four atoms), 171 ppm (twelve atoms), and 205 ppm (twelve atoms), as shown at “no CO₂” column on the right-end of Figure 5(b). The ¹³C NMR chemical shifts were experimentally observed at 129 ppm, 137 ppm, and 171 ppm and previously calculated at 130.8 ppm, 137.1 ppm, and 171.0 ppm by DFT using the PBE functional.⁶⁶ These were assigned to the aromatic carbon atom bound to the hydrogen atom, the aromatic ipso carbon atoms bound to the carboxyl (-COO) group, and the carbonyl carbon atoms, respectively. The ¹³C NMR shielding constants calculated here agree with the assignments of the former work⁶⁶ and the differences between these three NMR shielding constants are almost the same as those of the experimentally observed chemical shifts.⁶⁶ When one CO₂ molecule is adsorbed, the ¹³C NMR shielding constants of the adsorbed CO₂ molecule is calculated in the range 156–163 ppm; see the violin plot at the “I”, “II”, and “III” columns in Figure 5(b). The shielding constant below 165 ppm depends moderately on the CO₂ adsorption at Sites I, II, and III. When fifteen CO₂ molecules are adsorbed to UiO-66, the ¹³C NMR shielding constants at 165 ppm (due to carbons bound to hydrogens) broaden to a cluster of values in the interval of 165–170 ppm, respectively, as shown by the “15 CO₂” column at the left-end of Figure 5(b). Similarly, the peak initially at 171 ppm shifts broadens to an interval 173–175 ppm upon absorption. Although the violin plot and the mean values do not change very much upon adsorption of fifteen CO₂ molecules, the broadening of ¹³C NMR shielding constants around 165–170 ppm and 173–175 ppm can be used as a signal for full CO₂ adsorption.

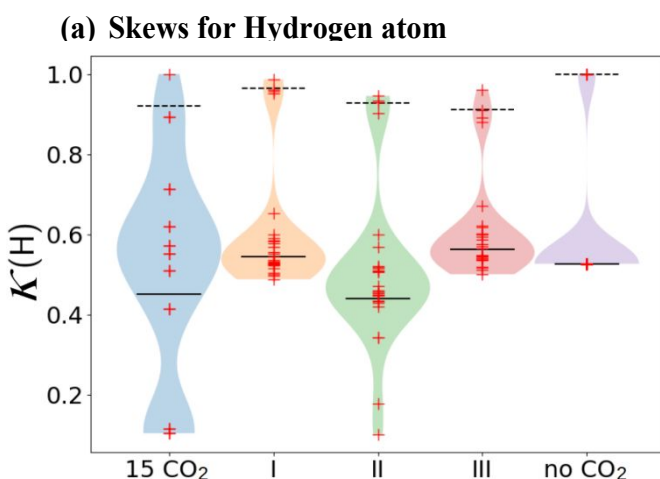
Oxygen shielding constants: The oxygen atoms in UiO-66 without CO₂ adsorption exhibit shielding constants around 66 ppm (one atom), 325 ppm (twenty-four atoms), and 459 ppm (two atoms), as shown at the right-end (the “no CO₂” column) of Figure 4(c). The peak at 66 ppm was not experimentally observed, but this is not unreasonable because only one oxygen atom contributes to it and the experimental signal should be very small. Adsorption of one CO₂ molecule at Sites I, II, and III slightly changes the peaks around 325 and 459 ppm and broadens the peak around 66 ppm to the interval 66–105 ppm; see the “I”, “II”, and “III” columns in Figure 5(c). When fifteen CO₂ molecules are adsorbed, the cluster around 100 ppm broadens, as

shown by the “15 CO₂” column at the left-end of Figure 5(c). In addition, the violin plot around 100 ppm changes considerably when fifteen CO₂ molecules are adsorbed. These results indicate that the ¹⁷O NMR spectroscopy is effective for studying CO₂ adsorption into UiO-66. Indeed, the ¹⁷O NMR measurement has been employed for investigating MOFs.⁶⁷

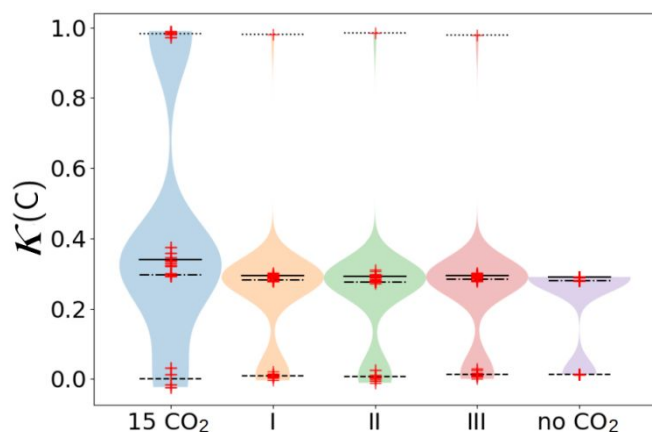
Shielding anisotropy: Adsorption of CO₂ also manifests itself in the anisotropy of the nuclear shielding tensor. With the conventional relation $\sigma_{11} > \sigma_{22} > \sigma_{33}$ for the eigenvalues of the nuclear shielding tensors, we define the skew by,⁶⁹

$$\kappa = 3 \frac{\sigma_{iso} - \sigma_{22}}{\sigma_{11} - \sigma_{33}} = \frac{\sigma_{11} + \sigma_{33} - 2\sigma_{22}}{\sigma_{11} - \sigma_{33}} \quad (5)$$

where either shielding constants or chemical shifts can be used. Although the isotropic value is important for the location of the NMR spectrum, the skew κ is important for the line shape. Extreme values of $\kappa = +1$ and $\kappa = -1$ indicate an asymmetrical peak with a heavy tail towards the right and left, respectively, while $\kappa = 0$ indicates a symmetric peak. In Figure 6, the distributions of this value are visualized as data points and as violin plots: All calculated skews are presented in the Supplementary Material Table S4.



(b) Skews for Carbon atom



(c) Skews for Oxygen atom

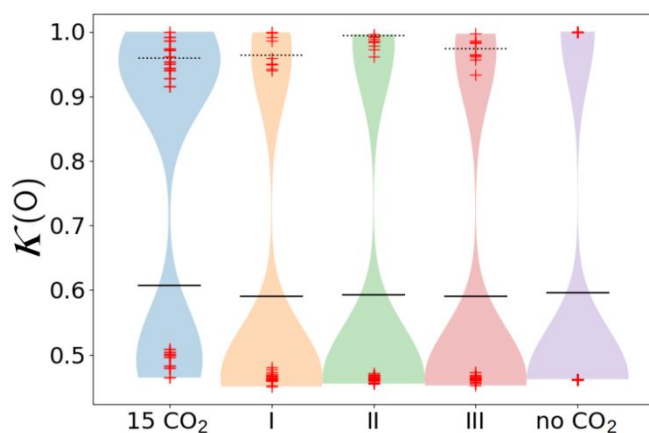


Figure 6: The skew of hydrogen (left), carbon (middle), oxygen (right) atoms in CO₂ with UiO-66. The leftmost distribution is for UiO-66 with fifteen CO₂. The next three are for one CO₂ at Site I, II, and III, respectively. The rightmost distribution is for UiO-66 without CO₂. Data points are shown as crosses. The horizontal solid, dashed, dash-dotted, and dotted lines show mean values for different chemical groupings of the atoms.

For the hydrogen atoms in the UiO-66 without CO₂ adsorption, all shielding tensors exhibit heavy tails in the right direction (most signals have $\kappa = 0.53$ and three have $\kappa = 1.0$), as shown in Figure

4(a) (right-end). A similar feature is observed when one CO₂ molecule is adsorbed at Site I or III. When one CO₂ molecule is adsorbed at Site II, however, several peaks exhibit smaller skew ($0 < \kappa < 0.5$). None of the proton peaks has negative skew. When fifteen CO₂ molecules are adsorbed, six new signals with skew near 0.1 appear, while the others mainly take on more intermediate values between the initial $\kappa = 0.5$ and $\kappa = 1.0$. These results suggest that CO₂ adsorption is difficult to detect via the skew of H signals, with the main effect of adsorption at Site III being the appearance of more symmetric peaks.

The anisotropy of the carbon NMR shielding constants in UiO-66 without CO₂ exhibits a smaller skew ($0 < \kappa < 0.3$) than does the hydrogen shielding constant (Figure 4(b); right-end). These values are consistent with the small skews of carbon NMR signals reported previously (Fig. 2a in Ref. 65). When one CO₂ molecule is adsorbed at Site I, II, or III, its carbon NMR shielding constants show very large skew around $\kappa \approx +1$ (Figure 4(b); middle results). This remains the same when fifteen CO₂ molecules are adsorbed (Figure 4(b); left-end). However, for the carbons in UiO-66, the skews are insensitive to adsorption of fifteen CO₂ molecules except for a moderate shift from 0.3 to around 0.35. On the other hand, the oxygen shielding constants of UiO-66 show both strongly positive and negative skews when no CO₂ adsorption occurs (Figure 4(c); right-end). They change little when one CO₂ molecule is adsorbed. When fifteen CO₂ molecules are adsorbed, however, the negative skew disappears and all peaks exhibit a strongly positive skew ($0.45 < \kappa < 1.0$), indicating that the heavy tail in the left direction disappears when fifteen CO₂ molecules are adsorbed. The violin plot clearly shows this change in skew (Figure 4(c); left-end).

In summary, the skews of carbon and oxygen NMR peaks change considerably upon the adsorption of fifteen CO₂ molecules, whereas the skews of hydrogen NMR peaks change moderately. NMR line shapes of carbon and oxygen atoms are useful for investigating CO₂ adsorption, although the carbon and oxygen NMR shielding constants are not very sensitive to CO₂ adsorption, as described above.

Conclusions.

In this work, we investigated adsorption of carbon dioxide, acetone, and methanol to UiO-66 using a CM/PM-combined method consisting of DFT calculation on infinite UiO-66 under periodic boundary condition and post-Hartree-Fock (SCS-MP2 and MP2.5) calculations on cluster models. The adsorption of fifteen to sixteen CO₂ molecules occurs at three sites. One molecule is adsorbed at each μ -OH group bridging three Zr atoms (Site I); in total, three or four CO₂ molecules are adsorbed at Site I, maybe depending on the pressure. Six CO₂ molecules are adsorbed around the pillar ligand, where each molecule is loosely surrounded by three terephthalate ligands (Site II). Further six molecules are adsorbed around the pillar ligand, where the gas molecule is surrounded well by three terephthalate ligands (Site III). Methanol and acetone are adsorbed at Site I, II, and III in the similar manner to CO₂. The adsorption energy decreases in the order Site I > Site III > Site II for all three gas molecules. The strongest adsorption occurs at Site I. At this site, the protonic hydrogen atom of the μ -OH group bridging three Zr atoms interacts with the oxygen atom of gas molecule through a Brønsted-acid–Lewis-base interaction. This is the reason why the particularly large adsorption energy is obtained at Site I. At Site I, the binding energy decreases in the order acetone > methanol > CO₂ because the negative charge of the oxygen atom decreases in the order acetone > methanol >> CO₂. This Site I is effective for adsorption of gas molecule with negatively charged atom and/or Lewis base moiety. At Sites II and III, the adsorption occurs by weak interactions; the electrostatic interactions of the oxygen atom of the gas molecule with the hydrogen atoms of the C₆H₄ ring and carboxyl carbon atom in the CO₂ adsorption, the CH- π interaction and electrostatic interaction between the methyl hydrogen atoms of the gas molecule and the oxygen atoms of the ligand in the acetone adsorption, and the OH- π interaction and the electrostatic interaction between the protonic hydrogen atom of the methanol OH group and the oxygen atoms of the carboxyl group of the ligand in the methanol adsorption.

The post-Hartree-Fock correction decreases the adsorption energy by 4 % at Site I when the HO-Zr moiety is involved in the correction, 9 % when the HO-Zr moiety is not involved in the correction, 29 % at Site II, and 11% at Site III in the CO₂ adsorption case. The correction of *BE* at Site I is small because the Brønsted-acid–Lewis-base interaction including the electrostatic interaction between the negatively charged oxygen atom of CO₂ and the positively charged hydrogen atom of the μ -OH group largely contributes to the adsorption energy at Site I. It is likely that the larger post-Hartree-Fock correction at Site II is attributable to the CO₂ adsorption structure in which the CO₂ exists at a rather short distance from the C₆H₄ ring of the terephthalate ligand but the CO₂ π orbitals deviate from that of the C₆H₄ ring; because such a deviated position leads to smaller dispersion and π - π interactions, post-Hartree-Fock methods are needed for a correct evaluation of the binding energy.

Because CO₂ adsorption to MOFs is a promising technique for CO₂ capture from combustion gases, we focus on to what extent NMR measurements of hydrogen, carbon, and oxygen atoms provide meaningful information on CO₂ adsorption. The isotropic shielding constant of the hydrogen atom significantly differs among adsorptions of no CO₂, one CO₂ (at Site I, II, or III), and fifteen CO₂ molecules (Sites I to III). Although the isotropic carbon and oxygen NMR measurements do not change very much by CO₂ adsorption, their skews depend on CO₂ adsorption, indicating that the carbon and oxygen NMR measurements are also useful for investigating the CO₂ adsorption. These results strongly suggest that NMR spectroscopy is a promising experimental tool for investigating CO₂ adsorption to UiO-66.

■ ASSOCIATED CONTENT

Supporting Information

The Supporting Information is available free of charge at <https://pubs.acs.org/doi/xxxx>. Comparison

of interaction energy of gas molecule with ligand moiety between SCS-MP2, MP2.5, and CCSD(T) (Table S1), $BE^{\text{MP2.5}}(\text{SCM-}i)$ and $BE^{\text{SCS-MP2}}(\text{SCM-}i)$ values (Table S2 and S3), all calculated NMR shielding constants (Table S4), all calculated skews (Table S5) (PDF).

■ AUTHOR INFORMATION

Corresponding Authors

Trygve Helgaker *Hylleraas Centre, Department of Chemistry, The Faculty of Mathematics and Natural Sciences, University of Oslo, Norway. Postboks 1033 0315 Oslo, Norway. Orcid org/0000-0002-5032-8392. Email: trygve.helgaker@kjemi.uio.no*

Shigeyoshi Sakaki *Institute for Integrated Cell-Material Sciences, Rohm Plaza R312, Kyoto University, Kyoto-Daigaku Katsura, Nishikyo-ku, Kyoto 615-8246, Japan. Orcid org/0000-0002-1783-3282. Email: sakaki.shigeyoshi.47e@st.kyoto-u.ac.jp*

Authors

Michiko Atsumi *Hylleraas Centre for Quantum Molecular Sciences, Department of Chemistry, University of Oslo, Box 1033, N-0315, Norway. Orcid org/0000-0003-3237-7278.*

Jia-Jia Zhong *Laboratory of Theoretical and Computational Nanoscience, CAS Center for Excellence in Nanoscience, National Center for Nanoscience and Technology, Chinese Academy of Sciences, No.11 Zhong Guan Cun Bei Yi Tiao, Beijing 100190, China. Orcid org/0000-0002-6040-6219.*

Erik Tellgren *Hylleraas Centre for Quantum Molecular Sciences, Department of Chemistry, University of Oslo, Box 1033, N-0315, Norway. Orcid org/0000-0002-0019-4330.*

Complete contact information is available at: <https://pubs.acs.org/>

Notes The authors declare no competing financial interest.

■ **ACKNOWLEDGMENTS** This work was supported by JST-CREST (JPMJCR20B6), JSPS Grant-in-aid for Scientific Research (JPJSBP1 20199902). We wish to thank Research Center for Computational Science in National Institutes of Natural Sciences (NINS), Okazaki, Japan for the use of Super Computers (Project: 22-IMS-C003), UNINETT Sigma2 - the National Infrastructure for High Performance Computing and Data Storage for providing computational resources, and the Center of Excellence Hylleraas Center for Quantum Molecular Sciences (Grant No. 262695) in Norway.

References

-
- (1) 1J. H. Cavka, S. Jakobsen, U. Olsbye, N. Guillou, C. Lamberti, S. Bordiga and K. P. Lillerud, *J. Am. Chem. Soc.*, 2008, **130**, 13850–13851.
 - (2) 2M. Kandiah, M. H. Nilsen, S. Usseglio, S. Jakobsen, U. Olsbye, M. Tilset, C. Larabi, E. A. Quadrelli, F. Bonino and K. P. Lillerud, *Chem. Mater.*, 2010, **22**, 6632–6640.
 - (3) 3L. Valenzano, B. Civalieri, S. Chavan, S. Bordiga, M. H. Nilsen, S. Jakobsen, K. P. Lillerud and C. Lamberti, *Chem. Mater.*, 2011, **23**, 1700–1718.
 - (4) 4M. Kandiah, S. Usseglio, S. Svelle, U. Olsbye, K. P. Lillerud and M. Tilset, *J. Mater. Chem.*, 2010, **20**, 9848–9851.
 - (5) 5S. Yuan, J. Qin, C. Lollar and H. Zhou, *Chem. Rev.*, 2014, **114**, 10575–10612.
 - (6) 6D. Zou and D. Liu, *Mater. Today Chem.*, 2019, **12**, 139–165.
 - (7) 7N. Hanikel, M. S. Prévot and O. M. Yaghi, *Nat. Nanotechnol.*, 2020, **15**, 348–355.
 - (8) 8M. Wu, Q. Zhang, Q. Zhang, H. Wang, F. Wang, J. Liu, L. Guo and K. Song, *Front.*

-
- Chem.*, 2022, **10**, 842894.
- (9) 9J. Winarta, B. Shan, S. M. McIntyre, L. Ye, C. Wang, J. Liu and B. Mu, *Cryst. Growth Des.*, 2019, **20**, 1347–1362.
- (10) 10 M. Usman, A. Helal, M. M. Abdelnaby, A. M. Alloush, M. Zeama and Z. H. Yamani, *Chem. Rec.*, 2021, **21**, 1771–1791.
- (11) 11 X. Feng, H. S. Jena, C. Krishnaraj, K. Leus, G. Wang, H. Chen, C. Jia and P. Van Der Voort, *ACS Applied Materials & Interfaces*, 2021, **13**, 60715–60735.
- (12) 12 F. Ahmadijokani, H. Molavi, M. Rezakazemi, S. Tajahmadi, A. Bahi, F. Ko, T. M. Aminabhavi, J.-R. Li and M. Arjmand, *Prog. Mater. Sci.*, 2022, **125**, 100904.
- (13) 13 S. Kitagawa, R. Kitaura and S.-i. Noro, *Angew. Chem., Int. Ed. Engl.*, 2004, **43**, 2334–2375.
- (14) 14 D. K. Wanigarathna, J. Gao and B. Liu, *Materials Advances*, 2020, **1**, 310–320.
- (15) 15 T. Wang, E. Lin, Y.-L. Peng, Y. Chen, P. Cheng and Z. Zhang, *Coord. Chem. Rev.*, 2020, **423**, 213485.
- (16) 16 J.-R. Li, R. J. Kuppler and H.-C. Zhou, *Chem. Soc. Rev.*, 2009, **38**, 1477–1504.
- (17) 17 T. Pham, K. A. Forrest, D. M. Franz and B. Space, *CrystEng-Comm*, 2017, **19**, 4646–4665.
- (18) 18 Z. Zhai, X. Zhang, X. Hao, B. Niu and C. Li, *Adv. Mater. Technol.*, 2021, **6**, 2100127.

-
- (19)19 H. R. Abid, H. Tian, H.-M. Ang, M. O. Tade, C. E. Buckley and S. Wang, *J. Chem. Eng.*, 2012, **187**, 415–420.
- (20)20 O. G. Nik, X. Y. Chen and S. Kaliaguine, *J. Membr. Sci.*, 2012, **413**, 48–61.
- (21)21 C. Chen, Y.-R. Lee and W.-S. Ahn, *Journal of nanoscience and nanotechnology*, 2016, **16**, 4291–4301.
- (22)22 J. Liu, P. K. Thallapally, B. P. McGrail, D. R. Brown and J. Liu, *Chem. Soc. Rev.*, 2012, **41**, 2308–2322.
- (23)23 S. Shalini, S. Nandi, A. Justin, R. Maity and R. Vaidhyanathan, *Chem. Commun.*, 2018, **54**, 13472–13490.
1. 24 L. Li, H. S. Jung, J. W. Lee and Y. T. Kang, *Renew. Sust. Energ. Rev.*, 2022, **162**, 112441.
2. 25 Y.-S. Bae and R. Q. Snurr, *Angew. Chem., Int. Ed. Engl.*, 2011, **50**, 11586–11596.
3. 26 H. Li and M. R. Hill, *Acc. Chem. Res.*, 2017, **50**, 778–786.
4. 27 H. Jasuja, J. Zang, D. S. Sholl and K. S. Walton, *J. Phys. Chem. C.*, 2012, **116**, 23526–23532.
5. 28 Q. Yang, S. Vaesen, F. Ragon, A. D. Wiersum, D. Wu, A. Lago, T. Devic, C. Martineau, F. Taulelle, P. L. Llewellyn, H. Jobic, C. Zhong, C. Serre, G. De Weireld and G. Maurin, *Angew. Chem., Int. Ed. Engl.*, 2013, **39**, 10316–10320.
6. 29 M. Younas, M. Reza kazemi, M. Daud, M. B. Wazir, S. Ahmad, N. Ullah,

-
- Inamuddin and S. Ramakrishna, *Prog. Energy Combust.*, 2020, **80**, 100849.
7. 30 H. Chevreau, W. Liang, G. J. Kearley, S. G. Duyker, D. M. D'Alessandro and V. K. Peterson, *J. Phys. Chem. C.*, 2015, **119**, 6980–6987.
8. 31 A. Nandy, A. C. Forse, V. J. Witherspoon and J. A. Reimer, *J. Phys. Chem. C.*, 2018, **122**, 8295–8305.
9. 32 Materials Studio. BIOVIA Inc., San Diego, California, USA.
10. 33 A. K. Rappé, C. J. Casewit, K. Colwell, W. A. Goddard III and W. M. Skiff, *J. Am. Chem. Soc.*, 1992, **114**, 10024–10035.
11. 34 A. K. Rappe and W. A. Goddard III, *J. Phys. Chem.*, 1991, **95**, 3358–3363.
12. 35 Q. Yang, D. Liu, C. Zhong and J.-R. Li, *Chem. Rev.*, 2013, **113**, 8261–8323.
13. 36 S. Zuluaga, P. Canepa, K. Tan, Y. J. Chabal and T. Thonhauser, *J. Condens. Matter Phys.*, 2014, **26**, 133002.
14. 37 J. P. Perdew, K. Burke and M. Ernzerhof, *Phys. Rev. Lett.*, 1996, **77**, 3865.
15. 38 S. Grimme, *J. Comput. Chem.*, 2004, **25**, 1463–1473.
16. 39 S. Grimme, J. Antony, S. Ehrlich and H. Krieg, *J. Chem. Phys.*, 2010, **132**, 154104.
17. 40 U. Ryde, R. A. Mata and S. Grimme, *Dalton Trans.*, 2011, **40**, 11176–11183.
18. 41 P. E. Blöchl, *Phys. Rev. B.*, 1994, **50**, 17953.
19. 42 G. Kresse and D. Joubert, *Phys. Rev. B.*, 1999, **59**, 1758.
20. 43 G. Kresse and J. Furthmüller, *Comput. Mater. Sci.*, 1996, **6**, 15–50.

-
21. 44 G. Kresse and J. Furthmüller, *Phys. Rev. B.*, 1996, **54**, 11169.
22. 45 K. Sillar and J. Sauer, *J. Am. Chem. Soc.*, 2012, **134**, 18354–18365.
23. 46 A. Kundu, G. Piccini, K. Sillar and J. Sauer, *J. Am. Chem. Soc.*, 2016, **138**, 14047–14056.
24. 47 J.-J. Zheng, S. Kusaka, R. Matsuda, S. Kitagawa and S. Sakaki, *J. Am. Chem. Soc.*, 2018, **140**, 13958–13969.
25. 48 C. Gu, N. Hosono, J.-J. Zheng, Y. Sato, S. Kusaka, S. Sakaki and S. Kitagawa, *Science*, 2019, **363**, 387–391.
26. 49 J.-J. Zheng and S. Sakaki, *J. Photochem. Photobiol. C: Photochem. Rev.*, 2022, **51**, 100482.
27. 50 S. Dapprich, I. Komáromi, K. S. Byun, K. Morokuma and M. J. Frisch, *J. Mol. Struct. (Theochem)*, 1999, **461**, 1–21.
28. 51 L. W. Chung, W. Sameera, R. Ramozzi, A. J. Page, M. Hatanaka, G. P. Petrova, T. V. Harris, X. Li, Z. Ke, F. Liu, H.-B. Li, L. Ding and K. Morokuma, *Chem. Rev.*, 2015, **115**, 5678–5796.
29. 52 S. Grimme, *J. Chem. Phys.*, 2003, **118**, 9095–9102.
30. 53 S. Grimme, *J. Phys. Chem. A*, 2005, **109**, 3067–3077.
31. 54 K. E. Riley, M. Pitonák, P. Jurecka and P. Hobza, *Chem. Rev.*, 2010, **110**, 5023–5063.
32. 55 M. M. Deshmukh and S. Sakaki, *J. Comput. Chem.*, 2012, **33**, 617–628.
33. 56 D. Andrae, U. Haeussermann, M. Dolg, H. Stoll and H. Preuss, *Theor. Chim.*

Acta, 1990, **77**, 123–141.

34. 57 S. F. Boys and F. Bernardi, *Mol. Phys.*, 1970, **19**, 553–566.
35. 58 M. J. Frisch, G. W. Trucks, H. B. Schlegel, G. E. Scuseria, M. A. Robb, J. R. Cheeseman, G. Scalmani, V. Barone, G. A. Peters- son, H. Nakatsuji, X. Li, M. Caricato, A. V. Marenich, J. Bloino, B. G. Janesko, R. Gomperts, B. Mennucci, H. P. Hratchian, J. V. Ortiz, A. F. Izmaylov, J. L. Sonnenberg, D. Williams- Young, F. Ding, F. Lipparini, F. Egidi, J. Goings, B. Peng, A. Petrone, T. Henderson, D. Ranasinghe, V. G. Zakrzewski, J. Gao, N. Rega, G. Zheng, W. Liang, M. Hada, M. Ehara, K. Toyota, R. Fukuda, J. Hasegawa, M. Ishida, T. Nakajima, Y. Honda, O. Kitao, H. Nakai, T. Vreven, K. Throssell, J. A. Montgomery, Jr., J. E. Peralta, F. Ogliaro, M. J. Bearpark, J. J. Heyd, E. N. Brothers, K. N. Kudin, V. N. Staroverov, T. A. Keith, R. Kobayashi, J. Normand, K. Raghavachari, A. P. Ren- dell, J. C. Burant, S. S. Iyengar, J. Tomasi, M. Cossi, J. M. Millam, M. Klene, C. Adamo, R. Cammi, J. W. Ochterski, R. L. Martin, K. Morokuma, O. Farkas, J. B. Foresman and D. J. Fox, *Gaussian 16 Revision A.03*, 2016, Gaussian Inc. Wallingford CT.
36. 59 (a) These $BE^{\text{PBE-D3:PBC}}$ values were calculated as a difference between the $BE^{\text{PBE-D3:PBC}}$ values for the adsorption of sixteen CO_2 molecules and that for fifteen CO_2 molecules. These values are larger than the $BE^{\text{PBE-D3:PBC}}$ value for one CO_2 molecule, which is discussed below and shown in Table 2. It is likely that the larger $BE^{\text{PBE-D3:PBC}}$ values result from the CO_2 - CO_2 van der Waals type attractive interactions. (b) The seventeenth CO_2 molecule is adsorbed at the new site. This site is distant from pillar ligand and the seventeenth CO_2 molecule is surrounded well by CO_2 molecules at site II. This new site is possible only here. It is likely suggested

that seventeen CO₂ molecules are adsorbed but the adsorption of more than seventeen CO₂ molecules is difficult to occur.

- 60 The powder sample was used for neutron powder diffraction (NPD) measurements followed by Rietveld refinement. See Ref. 30.
37. 61 The gas adsorption at Site III occurs with the dispersion interactions described below; the π - π interaction contributes to the CO₂ adsorption and the OH- π interaction contributes to the methanol adsorption. Although the CH bonds of methyl groups of acetone are considerably distant from the C₆H₄ ring, it is likely that the CH- π interaction contributes to the acetone adsorption because the CH bonds of two methyl groups exist at a good position for the CH- π interaction with the C₆H₄ ring.
- 62 C. H. Lau, R. Babarao and M. R. Hill, *Chem. Comm.*, 2013, **49**, 3634–3636.
38. 63 A. Policicchio, M. Florent, A. Celzard, V. Fierro, J. Jagiello and T. J. Bandoz, *Microporous Mesoporous Mater.*, 2020, **309**, 110571.
- 64 The experimental value was estimated to be about 26 kJ/mol from Figure 4 of Ref.62 and 22 kJ/mol from Figure 9 of Ref.63.
39. 65 H. Wu, Y. S. Chua, V. Krungleviciute, M. Tyagi, P. Chen, T. Yildirim and W. Zhou, *J. Am. Chem. Soc.*, 2013, **135**, 10525–105
40. 66 Y. Ma, W. Lu, X. Han, Y. Chen, I. Da Silva, D. Lee, A. M. Shevel-eva, Z. Wang, J. Li, W. Li, M. Fan, S. Xu, F. Tuna, Y. McInnes, Eric J. L. and Cheng, S. Rudi'c, P. Manuel, M. D. Frogley, A. J. Ramirez-Cuesta, M. Schröder and S. Yang, *J. Am. Chem. Soc.*, 2022, **144**, 8624–8632.

-
41. 67 S. Devautour-Vinot, G. Maurin, C. Serre, P. Horcajada, D. Paula da Cunha, V. Guillermin, E. de Souza Costa, F. Taulelle and C. Martineau, *Chem. Mater.*, 2012, **24**, 2168–2177.
42. 68 P. He, J. Xu, V. V. Terskikh, A. Sutrisno, H.-Y. Nie and Y. Huang, *J. Phys. Chem. C.*, 2013, **117**, 16953–16960.
43. 69 J. Mason, *Solid State Nucl. Magn. Reson.*, 1993, **2**, 285–288.